DOI: 10.18462/iir.gl2022.0036

# Self-sufficient Propane-CO2 cascade with two-phase thermosiphon - Simulation of an evaporating two-phase flow with variable heat transfer coefficient

**Oliver Schmid*[(a)], Tobias Nitschke[(a)],Elena Melito[(a)], Sebastian Gund [(a)], Prof. Dr.-Ing. Habil. Michael Kauffeld [(a)]**

[(a)] Institute of refrigeration, air conditioning and environmental engineering
Karlsruhe, 76133, Germany, mailbox@h-ka.de
*Corresponding author: oliver.schmid@h-ka.de

## ABSTRACT

A thermal energy storage (ice storage) is to be charged by a natural circulation evaporator, also called a two-phase thermosiphon. When using the natural circulation evaporator, the heat transmittance coefficient from the freezing water to the refrigerant changes with the loading of the ice storage. For the correct design of such a system it is important to predict the pressure drop and the flow behavior. In order to use a minimum of refrigerant, the smallest pipe diameter should be calculated at which the thermosiphon can be operated even with the required ice thickness on the outside. In this paper, a simulation is described, whereby the flow patterns, the required pipe length and the pressure drop can be determined for different internal pipe diameters and increasing ice thickness. A variable length pipe coil is simulated. R-744 (carbon dioxide) is used as refrigerant. The design procedure is explained by means of an example application in which an ice storage system is calculated for a cascade refrigeration system inside a refrigerated container.

Keywords: Refrigeration, Carbon Dioxide, Thermosiphon, Energy Efficiency.

## 1. INTRODUCTION

Due to a rising world population, a higher standard of living and, not least, climate change, the global demand for cooling and air conditioning will continue to increase in the coming years. On the African continent in particular, demand for air-conditioning equipment will increase fourfold by 2040 (IEA 2019). In addition, forecasts predict that the African continent is likely to host more than half of the expected global population growth between 2015 and 2050. This is in contrast to poor electrical infrastructure and unreliability of grid stability in many African countries, especially in the sub-Saharan region. With the prevailing high temperatures, a continuous cold chain of food and medicines is essential. However, in sub-Saharan Africa, about 26% of the more than 100,000 health facilities are not electrified (Maina et al. 2019). 28% do not have reliable electrical power. Although this area has tremendous potential for renewable energy, particularly through photovoltaics, large parts of this region do not have a power grid. In the event of a power outage, cheap diesel generators continue to step in. The EU project SophiA (Sustainable off-grid solution for Pharmacies and Hospitals in Africa) will construct an environmentally friendly alternative for storage at different temperature levels (+5 °C, -30 °C and -70 °C). The application will be tested for hospitals in four different climatic regions in Africa. A two-stage refrigeration cascade with thermal energy storage will be installed in a 40-foot container. The upper stage uses propane (R-290) as the refrigerant, while the lower stage uses CO2 (R-744) as the refrigerant. The phase change from water to ice is used as thermal energy storage. The ice storage is charged by means of a natural circulation evaporator, also called a thermosiphon. The circulation of the refrigerant takes place due to the difference in density between the supplied liquid refrigerant and the discharged gaseous refrigerant. The driving factor of the thermosiphon is the height difference to the liquid reservoir above. The thermosiphon has an influence on the arrangement of the components and size of the entire refrigeration system, which is why this simulations are carried out. The -70 °C storage temperature is ensured by separate freezers in the -30 °C room and will not be discussed further in this paper.

## 2. DESIGN OF A TWO PHASE THERMOSIPHON

The use of the natural refrigerants propane (R-290) and CO2 (R-744) is increasing due to the current "phase down" of halogenated refrigerants (Kauffeld et al. 2022). This can be justified by the thermodynamic properties of both refrigerants. Since R-744 has a high specific enthalpy and thus low mass flows have to be transported, the compressors require less installation space. In addition, both refrigerants have a low GWP and an ODP of 0. However, R-290 is flammable and the use of large charge volumes is regulated by strict regulations, which mean higher investment costs for the refrigeration system. R-744 has the disadvantage that the system must be operated transcritically at low efficiency and higher pressures at high ambient temperatures in the sub-Saharan region. In combination of R-290 and R-744 in a refrigerant cascade, the advantages of both refrigerants are used and the disadvantages become less effective. The first stage of the refrigeration system, operated with R-290, is kept compact, which reduces the charge. A cascade heat exchanger condenses the R-744 below the critical pressure. The liquid R-744 refrigerant is collected in a high-pressure receiver. In addition to the secondary R-744 refrigerant circuit, a natural circulation evaporator (two-phase thermosiphon) is connected in parallel to charge the ice storage (see Figure 1.1).

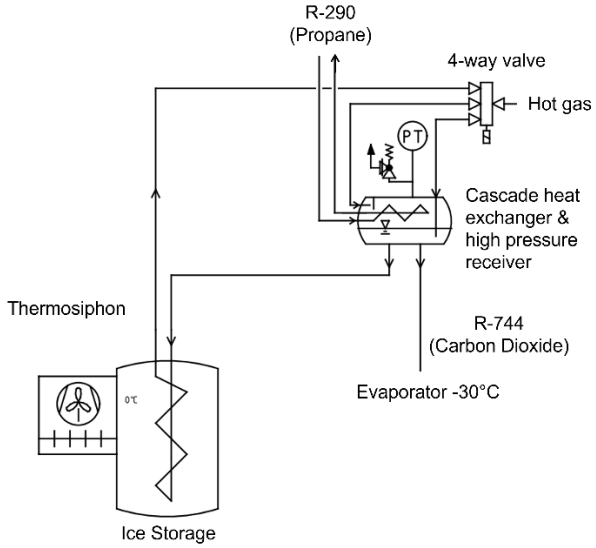


**Figure 1.1: P&ID of parallel thermosiphon**

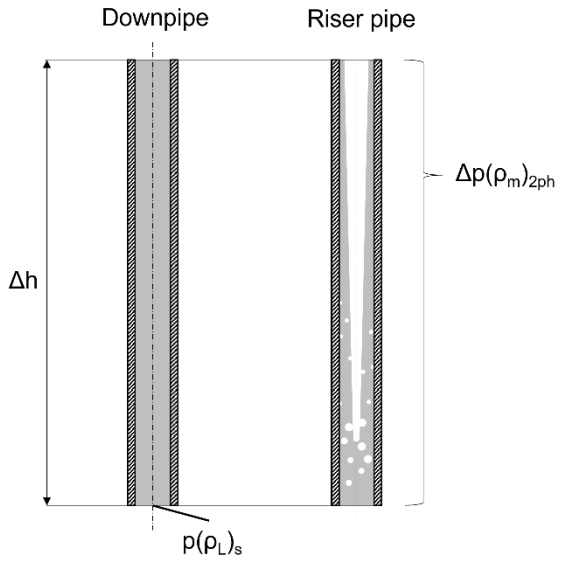


**Figure 1.2: Simplified workwise of a thermosiphon**

Since the refrigeration system operates only by the sustainable power supply from photovoltaics, the energy generated during the day must be stored for the night. A thermal storage system in the form of an ice storage tank is used for this purpose. The cooling of the +5 °C room is achieved passively by the ice storage, which is located in the room to be cooled. The ice storage is charged by the natural circulation evaporator as soon as the propane refrigeration system generates a greater cooling capacity than the CO2 refrigeration system requires for condensation. During nighttime operation, the upper stage of the cascade is shut down. In this mode of operation, the condensation of R-744 takes place via the same pipe coils of the ice storage tank, which is no longer operated as a thermosiphon. In the following, it is important to properly design the thermosiphon's coils. Natural circulation is achieved when the static pressure of the liquid refrigerant in the supply $p_s$ in Pa is greater than the pressure drop in the thermosiphon $\Delta p_{2ph}$ in Pa (Strauss 2016) (see Figure 1.2). Therefore, the pressure drop has an influence on the required height difference between the cascade heat exchanger and the high pressure receiver. Accordingly, the driving pressure drop pressure difference $\Delta p_{imp}$ must assume a value greater than 0.

$$\Delta p_{imp} = p_s - \Delta p_{2ph} > 0 \quad \text{Eq. (1)}$$

With:

$$p_S = \rho_L \cdot g \cdot h_{Coil,total} - \Delta p_{friction,h} \quad \text{Eq. (1.1)}$$

Here $\rho_L$ in $\mathrm{kg/m^3}$ is the density of the liquid, g in $\mathrm{m/s^2}$ is the acceleration due to gravity, and $h_{Coil,total}$ in m is the height of the pipe coil. The pipe friction $\Delta p_{friction,h}$ in Pa counteracts the static pressure and must therefore be subtracted from the total static pressure.

### 2.1. Design calculation of a thermosiphon

After the requirements for the refrigeration system and the load profile of the rooms to be cooled have been determined, the total amount of heat per day ($\mathrm{Q_{total}}$ in J) can be calculated. In addition to the amount of heat to be removed daily from the normal cold room at +5 °C ($\mathrm{Q_{req,+5°C}}$ in J) and the freezer room at -30 °C ($\mathrm{Q_{req,-30°C}}$ in J), the amount of heat from the thermal energy storage $\mathrm{Q_{ice}}$ in J must be taken into account. The heat quantity of the thermal energy storage just corresponds to the heat of crystallization, which is needed for the phase change of the water mass to ice. The amount of heat to be removed daily from the container is calculated as:

$$Q_{total} = Q_{ice} + Q_{req,+5°C} + Q_{req,-30°C} \quad \text{Eq. (2)}$$

This amount of heat must be transported out of the container during the course of the day, with only eight hours available for the provision of electrical energy. During this time, enough ice must be built up to compensate for the amount of heat from the freezer room during the night. The heat from the normal cold room is made possible by the passive cooling of the ice storage in the room. As a result, the amount of heat for the entire day must be removed from the thermosiphon. In addition, the storage tank should be loaded with ice in case not enough energy can be provided by photovoltaics the following day. The averaged heat flow of the thermosiphon ($\dot{Q}_{Thermosiphon}$) is calculated by the amount of heat produced in the available time ($\mathrm{t_{day}}$ in sec).

$$\dot{Q}_{Thermosiphon} = \frac{Q_{req,+5°C} + \dot{Q}_{-30°,night} \cdot (24 - t_{day}) + Q_{ice}}{t_{day}} \quad \text{Eq. (3)}$$

The heat flow $\dot{Q}_{Thermosiphon}$ calculated by Eq. 3 must be transferable by the thermosiphon. As the ice thickness increases, the heat transfer coefficient decreases sharply. The heat transfer coefficient in turn has an influence on the flow behavior of the evaporating refrigerant. The existing flow pattern of the refrigerant, as well as the pressure losses and the required pipe length are determined by the equations described below.

#### 2.1.1. Flow shape

According to chapter H3 in the VDI Heat Atlas (Kind 2013), the flow shape in the evaporator tubes must first be determined. The seven different flow forms bubble flow, plug flow, layer flow, wave flow, surge flow, ring flow and fog flow are distinguished. Depending on the flow form, different pressure losses and heat transfer coefficients from the inner pipe wall to the refrigerant are achieved. The assumption is made that no refrigerant evaporates until it enters the thermosiphon, which corresponds to a vapor mass fraction ($\dot{x}$ dimensionsless) of 0. In addition, an approximately horizontal pipe is assumed for the calculation of the flow regime, since the thermosiphon designed as a tube coil with a small pitch h in m, a large diameter $D_{Coil}$ in m, which means that the pitch angle Θ in ° is less than 10 °. $\dot{m}_{G/L}$ is the refrigerants mass flow in kg/s of the respective phase G for vapor and L for liquid.

$$\dot{x} = \frac{\dot{m}_G}{\dot{m}_L + \dot{m}_G}$$ Eq. (4)

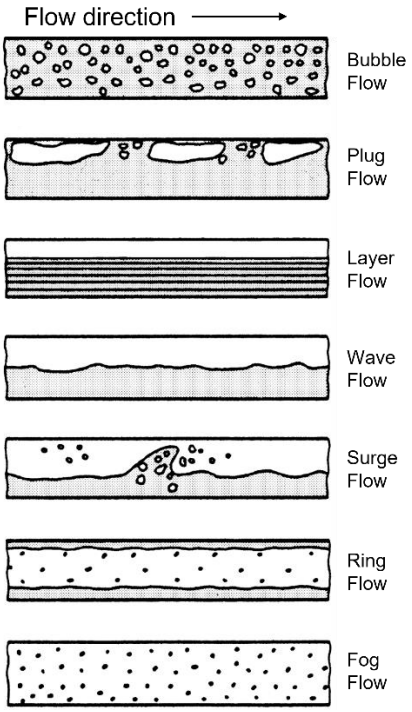


**Figure 2.1: Flow shapes in horizontal pipes (Kind 2013)**

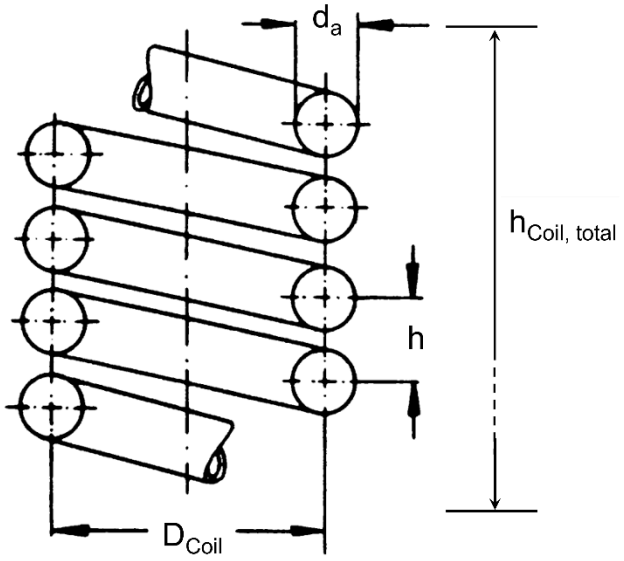


**Figure 2.2: Coil example (Gnielinski 2013)**

From the geometry of the assumed coil, the pitch angle Θ and the dimensionless value of the critical Reynolds number $Re_{crit}$ can already be calculated.

$$\Theta = arctan\left(\frac{h}{2 \cdot D_{Coil}}\right)$$ Eq. (5)

$$Re_{crit} = 2300\left[1 + 8.6\left(\frac{d_a}{D_{Coil}}\right)^{0.45}\right]$$ Eq. (6)

For the simulation, the coil is discretized into $\dot{x}_i$ sections of the vapor mass fraction (see section 2.2). All the following equations are calculated for a pipe segment of length $l_k$ in m, which is described in Eq. (23). To determine which flow shape is present, the Martinelli parameter (X, dimensionless) is calculated first,

$$X = \left(\frac{1 - \dot{x}}{\dot{x}}\right)^{0.875}\left(\frac{\rho_G}{\rho_L}\right)^{0.5}\left(\frac{\eta_L}{\eta_G}\right)^{0.125}$$ Eq. (7)

where $\dot{x}$ is the dimensionless vapor mass fraction, ρ is the density in $\mathrm{kg/m^3}$, and η in $\mathrm{kg/(m \cdot s)}$ is the dynamic viscosity of the respective phase (indices G for gas and L for liquid) (Martinelli 1948).

Furthermore, the following dimensionless quantities must be calculated. These quantities describe the boundary line at which a new flow form is established. On the basis of the comparison of the present case with the boundary lines in equations Eq. (18.1) to Eq. (18.6), the existing flow form is determined. Where $\dot{m}$ is the mass flow density in $\mathrm{kg/(m^2 s)}$, $\dot{x}$ is the dimensionless vapor mass fraction, Θ in ° is the angle of inclination of the pipe helix, d in m is the internal diameter of the pipe, g in $\mathrm{m/s^2}$ the acceleration due to gravity, η in $\mathrm{kg/(m \cdot s)}$ the dynamic viscosity, ξ the dimensionless pressure drop coefficient, σ in $\mathrm{kg/s^2}$ the surface tension, and ρ in $\mathrm{kg/m^3}$ the density of the respective phase.

$$Re_L Fr'_G = \frac{\dot{m}^3 \cdot \dot{x}^2 \cdot (1-\dot{x})}{\rho_G(\rho_L - \rho_G) \cdot \eta_L \cdot g \cdot cos\,\Theta} \quad \text{Eq. (8)}$$

$$Fr_{Gm} = \frac{\dot{m}^2 \cdot \dot{x}^2}{g \cdot d \cdot \rho_L \cdot \rho_G} \quad \text{Eq. (9)}$$

$$(FrEu)_L^{0.5} = \left(\frac{\xi_L \cdot \dot{m}^2 (1-\dot{x})^2}{2d \cdot \rho_L \cdot (\rho_L - \rho_G) \cdot g \cdot cos\,\Theta}\right)^{0.5} \quad \text{Eq. (10)}$$

With:

$$\xi_L = \frac{0.3164}{Re_L^{0.25}} \quad \text{Eq. (10.1)}$$

$$Re_L = \frac{\dot{m}(1-\dot{x}) \cdot d}{\eta_L} \quad \text{Eq. (10.2)}$$

$$\left({We}/{Fr}\right)_L = \frac{g \cdot d^2 \cdot \rho_L}{\sigma} \quad \text{Eq. (11)}$$

Since the tube is inclined by the angle Θ, further quantities must be determined, which depend on the liquid level $h_{surf}$ in m in the tube segment under consideration (see Figure 3). VDI heat atlas chapter H3.1 "Flow forms in evaporator tubes" suggest that the averaged density is determined with the dimensionless vapor volume fraction ε according to Rouhani (1969). This factor establishes a relationship between the flow vapor content ẋ and the filling level. In addition to the density of the gas phase $\rho_G$ and the liquid $\rho_L$ in $\mathrm{kg/m^3}$, the surface tension σ in $\mathrm{kg/s^2}$ , the acceleration due to gravity g in $\mathrm{m/s^2}$, and the mass flow density ṁ in $\mathrm{kg/(m^2 s)}$ are required. Thereupon, the angle τ in rad can be determined iteratively via Eq. (13). As an iterative solution method, the Newton method is used, which is not detailed in this work.

$$\varepsilon = \frac{\dot{x}}{\rho_G}\left[\left(1+0.12(1-\dot{x})\right)\left(\frac{\dot{x}}{\rho_G}+\frac{1-\dot{x}}{\rho_L}\right) + \frac{1.18(1-\dot{x})\left(g\sigma(\rho_L-\rho_G)\right)^{0.25}}{\dot{m}{\rho_L}^{0,5}}\right]^{-1} \quad \text{Eq. (12)}$$

$$\tau = 2 \cdot \pi \cdot \varepsilon + sin\,(\tau) \quad \text{Eq. (13)}$$

The relative liquid height $\tilde{h}_{L,0}$ is calculated approximately via the angle τ and the vapor volume fraction ε. Figure 3 illustrates the relationship between the vapor mass fraction ẋ and the liquid height $h_{pipe}$ in m.

$$\tilde{h}_{L,0} = h_{surf}/d_{pipe} \quad \text{Eq. (14)}$$

$$\tilde{h}_{L,0} = \frac{15\pi \cdot (1-\varepsilon)}{8 \cdot \left(3 \cdot \sin\left(\frac{\tau}{2}\right) + \sin\left(\frac{\tau}{4}\right)\right)}$$

Figure 3 also shows the geometric relationship for calculating the cross-sectional area of the liquid. If the pipe is more than half filled with liquid (liquid height $h_{pipe} > r_{pipe}$), the area of the triangle with the height $x_{surf}$ is added to the area of the circle section. Below a height $h_{pipe} < r_{pipe}$, the area of the triangle must be

subtracted. Therefore, to calculate the following dimensionless values, a distinction is made between the cases $\tilde{h}_{L,0} \leq 0.5$ and $\tilde{h}_{L,0} > 0.5$.

In the range $0 \leq \tilde{h}_{L,0} \leq 1$:

$$\tilde{U}_i = 2 \cdot \sqrt{\tilde{h}_L(1 - \tilde{h}_L)} \qquad \text{Eq. (15)}$$

For $\tilde{h}_L \leq 0.5$:

$$\psi = 2\pi - \tau \qquad \text{Eq. (16.1)}$$

$$\tilde{U}_L = \psi/2 \qquad \text{Eq. (16.2)}$$

$$\tilde{U}_G = \pi - \tilde{U}_L \qquad \text{Eq. (16.3)}$$

$$\tilde{f}_L = (\psi - sin(\psi))/8 \qquad \text{Eq. (16.4)}$$

$$\tilde{f}_G = \frac{\pi}{4} - \tilde{f}_L \qquad \text{Eq. (16.5)}$$

For $\tilde{h}_L > 0.5$:

$$\tilde{U}_G = \tau/2 \qquad \text{Eq. (17.1)}$$

$$\tilde{U}_L = \pi - \tilde{U}_G \qquad \text{Eq. (17.2)}$$

$$\tilde{f}_G = (\tau - sin(\tau))/8 \qquad \text{Eq. (17.3)}$$

$$\tilde{f}_L = \frac{\pi}{4} - \tilde{f}_G \qquad \text{Eq. (17.4)}$$

The calculated values from Eq. (7) to Eq. (11) must be compared with the dimensionless values Eq. (16.1) to Eq. (17.4), whereby it is important to keep the order. As soon as a condition is fulfilled, the comparison of the simulation stops.

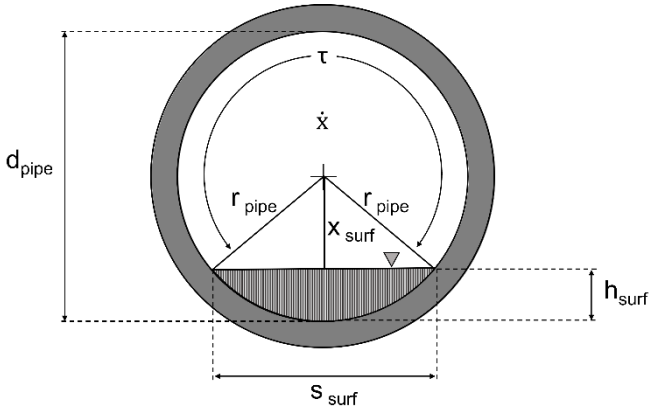


**Figure 3: Proportions in a circular tube (VDI Wärmeatlas p.901)**

Layer Flow:

$$Re_L Fr'_G \leq \frac{(226.3)^2}{\pi^3} \tilde{f}_L \cdot \tilde{f}_G^2 \quad \text{Eq. (18.1)}$$

Wave Flow:

$$Fr_{Gm} \leq \frac{16 \cdot \tilde{f}_G^2}{\pi^2 \sqrt{1-\left(2 \cdot \tilde{h}_L - 1\right)^2}} \cdot \left[\frac{\pi^2}{25 \cdot \tilde{h}_L^2} \cdot \left(\frac{Fr}{We}\right)_L + \frac{1}{cos(\Theta)}\right] = (Fr_{Gm})_{tt,Gr1} \quad \text{Eq. (18.2)}$$

Bubble Flow:

$$(FrEu)_L \geq \frac{128 \cdot \tilde{f}_G \cdot \tilde{f}_L^2}{\pi^2 \cdot \widetilde{U}_i} \quad \text{Eq. (18.3)}$$

Plug / Surge Flow:

If $X \geq 0.34,\ Re_L \geq 1187\ and\ Re_G\ \geq 1187$: Eq. (18.4)

$Fr_{Gm} > (Fr_{Gm})_{tt,Gr1}$

If $X \geq 0.51,\ Re_L \geq 1187\ and\ Re_G < 1187$:

$Fr_{Gm} > (Fr_{Gm})_{tt,Gr1}$

Fog Flow:

If $X \geq 0.51$ Eq. (18.5)

$$Fr_{Gm} \geq \frac{7680 \cdot \tilde{f}_G^2}{\pi^2 \cdot \xi_{Ph}} \cdot \left(\frac{Fr}{We}\right)_L = (Fr_{Gm})_{tt,Gr2}$$

With:

$$\xi_{Ph} = \left[1.138 + 2 \cdot log\left(\frac{\pi}{1.5 \cdot \tilde{f}_L}\right)\right]^{-2}$$

Ring Flow:

If $X < 0.51$ Eq. (18.6)

$(Fr_{Gm})_{tt,Gr1} \leq Fr_{Gm} \leq (Fr_{Gm})_{tt,Gr2}$

If none of the conditions is fulfilled, the simulation will give an error for this segment.

### 2.1.2. Pressure drops in evaporator tubes

The pressure loss of a two-phase flow ($\Delta p_{2ph}$ in Pa) in evaporator tubes is composed of friction pressure loss ($\Delta p_{friction}$ in Pa), static pressure loss ($\Delta p_{stat}$ in Pa) and acceleration pressure loss ($\Delta p_{acc}$ in Pa).

$$\Delta p_{2ph} = \Delta p_{friction} + \Delta p_{stat} + \Delta p_{acc} \quad \text{Eq. (19)}$$

Friction pressure loss

The method used to calculate the friction pressure loss $\Delta p_{friction}$ in Pa in the pipe section is described in chapter L "Two-phase gas-liquid flows" in the VDI Heat Atlas. The friction pressure loss is caused by the friction of the two phases against each other. The parameters in Table 1 are used for the calculation. In this table, the previously determined flow shapes are distinguished and parameters are assigned to them, which are required for the empirical friction pressure loss calculation according to Garcia et al (2003).

$$\Delta p_{friction} = \frac{l \cdot 2\rho_M \cdot w_M^2}{D} \cdot \left( a_2 \cdot Re^{b2} + \frac{(a_1 \cdot Re^{b1} - a_2 \cdot Re^{b2})}{\left(1 + \left(\frac{Re}{t}\right)^c\right)^d} \right) \quad \text{Eq. (20)}$$

With:

$$\rho_M = \rho_L \cdot \lambda_L + \rho_G \cdot (1 - \lambda_L) \quad \text{Eq. (20.1)}$$

$$\lambda_L = \frac{\dot{V}_L}{\dot{V}_L + \dot{V}_G} \quad \text{Eq. (20.2)}$$

$$Re = \frac{w_M \cdot D \cdot \rho_L}{\eta_L} \quad \text{Eq. (20.3)}$$

$$w_M = w_G + w_L \quad \text{Eq. (20.4)}$$

Where:

$$w_G = \frac{\dot{V}_G}{A} \quad \text{Eq. (20.5)}$$

$$w_L = \frac{\dot{V}_L}{A} \quad \text{Eq. (20.6)}$$

**Table 1: Parameters of gas-liquid fanning friction factor for different flow types (Wellenhofer 2013)**

| Parameter | a1 | b1 | a2 | b2 | c | d | t |
|---|---|---|---|---|---|---|---|
| Surge flow | 13,98 | –0,9501 | 0,1067 | –0,2629 | 3,577 | 0,2029 | 293 |
| Bubble flow | 13,98 | –0,9501 | 0,1067 | –0,2629 | 2,948 | 0,2236 | 304 |
| Layer flow | 13,98 | –0,9501 | 0,0445 | –0,1874 | 9,275 | 0,0324 | 300 |
| Ring flow | 3,671 | 0,6257 | 0,027 | –0,1225 | 2,191 | 0,2072 | 1000 |
| Other flows | 13,98 | -0,9501 | 0,0925 | -0,2534 | 4,864 | 0,1972 | 293 |

For the calculation, the mean empty pipe velocity $w_M$ in $m/s$, is first calculated from the respective single-phase fluid velocity $w_L$ in $m/s$ and the gas velocity $w_G$ in $m/s$. The corresponding Reynolds number is determined for this empty pipe velocity. The dimensionless factor $\lambda_L$ describes the ratio of the volumetric flow rate of the liquid phase $\dot{V}_L$ in $m^3/s$ to the total volumetric flow rate. $\rho_M$ is the average density of the considered two-phase flow in $kg/m^3$ , which is calculated from the single-phase densities of the substance (density of the liquid phase $\rho_L$ in $kg/m^3$ and gas phase $\rho_L$ in $kg/m^3$) with the dimensionless specific volume $\lambda_L$. Here, the variable l in m is the length (see Eq. (23)) and D in m is the diameter of the tube.

Static pressure drop

Due to the difference in height from inlet to outlet, a static pressure loss occurs. This is calculated by the general formula for static pressure:

$$\Delta p_{stat} = \rho_{total} \cdot g \cdot h_{section} \quad \text{Eq. (21)}$$

With:

$$\rho_{total} = \rho_L(1-\varepsilon) + \rho_G \cdot \varepsilon \quad \text{Eq. (21.1)}$$

$$h_{section} = \Delta l \cdot sin(\Theta) \quad \text{Eq. (21.2)}$$

Here, Δl in m corresponds to the length of the considered pipe section and the gradient angle Θ in ° described in section 2.1.1. As with the frictional pressure drop, the averaged density $\rho_{total}$ in Pa in the pipe section is determined by the ratio of the two single-phase densities. This factor is already required for the calculation of the flow shapes (see Eq. (12)).

Acceleration pressure loss

The evaporating refrigerant expands and thus counteracts the flow. This is taken into account by the acceleration pressure loss $\Delta p_{acc}$ in Pa. If the mean flow velocity is known, the acceleration pressure can be calculated with sufficient accuracy by the method presented in the VDI Heat Atlas chapter H3.2. For this, the mass flow density $\dot{m}$ in $kg/(m^2 s)$, the single-phase densities $\rho_L$ in $kg/m^3$ and $\rho_G$ in $kg/m^3$, the dimensionless vapor volume fraction ε and the vapor mass fraction at the inlet $\dot{x}_1$ and at the outlet $\dot{x}_2$ are required.

$$\Delta p_{acc} = \dot{m}^2 \left| \frac{\dot{x}^2}{\varepsilon \cdot \rho_G} + \frac{(1-\dot{x})^2}{(1-\varepsilon) \cdot \rho_L} \right|_{\dot{x}_1}^{\dot{x}_2} \quad \text{Eq. (22)}$$

### 2.1.3. Determination of tube length

In addition to the total pressure drop, the length $l_k$ in m of the pipe section under investigation is to be determined. The length is calculated by the heat transfer area A in $m^2$ required for the average heat flux $\dot{Q}_{Ice}$ in W, according to Péclet for multilayer cylinder jackets. The temperature at the ice formation front $T_{ice}$ is assumed constant at 273.15 K, while the evaporation temperature $T_{0,i,R744}$ in K changes due to the pressure drop. Accordingly, the temperature difference ΔT in K increases with increasing tube length. Due to the change in the vapor volume fraction ε, the flow velocity of the two-phase flow $c_{2ph}$ changes at constant mass flow. This in turn affects the average heat transfer coefficient $\alpha_{i,R744}$ in $W/(m^2K)$ between the refrigerant and the inside of the tube. Values which change with increasing tube length are marked with the index i (see Figure 4).

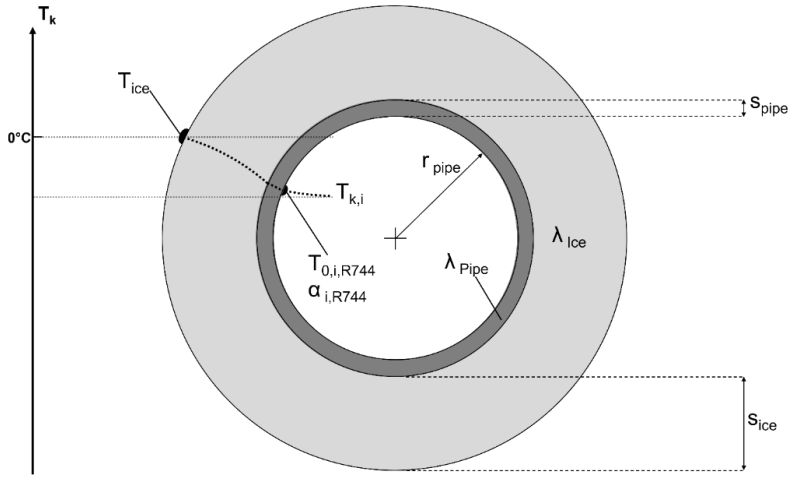


**Figure 4: Temperature profile $T_{k,i}$ of ice on pipe surface**

$$l_{i,k} = \frac{\dot{Q}_{i,Ice} \cdot K_{i,Péclet}}{2\pi \cdot \Delta T} \quad \text{Eq. (23)}$$

With:

$$\dot{Q}_{i,Ice} = \dot{Q}_{Ice} \cdot \Delta \dot{x} \quad \text{Eq. (23.1)}$$

$$K_{Péclet} = \frac{1}{\alpha_{i,R}} + \left(\frac{1}{\lambda_{Ice}} ln \frac{(r_{pipe} + s_{pipe} + s_{ice})}{(r_{pipe} + s_{pipe})}\right) + \left(\frac{1}{\lambda_{pipe}} ln \frac{(r_{pipe} + s_{pipe})}{(r_{pipe})}\right) \quad \text{Eq. (23.2)}$$

Here, the heat transfer coefficients $\lambda_{ice}$ and $\lambda_{pipe}$ in $\mathrm{W/(m \cdot K)}$ are constant material parameters of the ice and the pipe. In order to determine the heat transfer coefficient $\alpha_{i,R744}$ on the inside of the pipe, three cases have to be distinguished according to chapter G3 "Flow-through pipe spirals" in the VDI Heat Atlas (Gnielinski 2013): Heat transfer in laminar flow ($Re < Re_{crit}$), heat transfer in turbulent flow ($Re > 2{,}2 \cdot 10^4$) and heat transfer in the transition region ($Re_{crit} < Re < 2.2 \cdot 10^4$). The Nusselt correlations are listed for each of these three cases. $Re_{crit}$ is determined according to Eq. (6).

For the laminar flow region ($Re < Re_{crit}$), the following applies:

$$Nu_1 = \left(3.66 + 0.08\left[1 + 0.8\left(\frac{d_a}{D_{Coil}}\right)^{0.9}\right] Re^m \cdot Pr^{1/3}\right)\left(\frac{Pr}{Pr_w}\right)^{0.14} \quad \text{Eq. (24)}$$

With:

$$m = 0.5 + 0.02903\left(\frac{d}{D}\right)^{0.194} \quad \text{Eq. (24.1)}$$

Furthermore, for the turbulent region ($Re > 2.2 \cdot 10^4$), the following Nusselt correlation according to Schmidt (Schmidt 1967) is proposed:

$$Nu_t = \frac{\frac{\xi}{8} Re\ Pr}{1 + 12.7\sqrt{\frac{\xi}{8}}(Pr^{\frac{2}{3}} - 1)}\left(\frac{Pr}{Pr_w}\right)^{0{,}14} \quad \text{Eq. (25)}$$

With:

$$\xi = \frac{0{,}3164}{Re^{0.25}} + 0{,}03\left(\frac{d_a}{D_{Coil}}\right)^{0.5} \quad \text{Eq. (25.1)}$$

For the transition region ($Re_{crit} < Re < 2.2 \cdot 10^4$), linear interpolation between the respective Nusselt numbers at Rekrit and $Re = 2.2 \cdot 10^4$ is used, which according to Gnielinski (2013) is sufficient for accurate results. The critical Reynolds number is substituted into Eq. (24) for laminar flow, while turbulent flow with Reynolds number $Re = 2.2 \cdot 10^4$ is calculated according to Eq. (25) is calculated.

$$Nu = \gamma \cdot Nu_1(Re_{krit}) + (1 - \gamma) \cdot Nu_t(Re = 2.2 \cdot 10^4) \quad \text{Eq. (26)}$$

With:

$$\gamma = \frac{2.2 \cdot 10^4 - Re}{2.2 \cdot 10^4 - Re_{krit}} \qquad \text{Eq. (26.1)}$$

The distinction takes place for both the pure gas phase and the pure liquid phase, at point i. Then, the heat transfer coefficient $\alpha_{G/L}$ in W/(m²·K) of the pure phase can be calculated, where $\lambda_{G/L}$ in $\mathrm{W/(m \cdot K)}$ corresponds to the thermal conductivity of the gas or liquid phase. The characteristic length L corresponds to the inner diameter $d_{pipe,a}$ in m of the tube.

$$\alpha_{G/L} = \frac{\lambda_{G/L}}{d_i} \cdot Nu_{G/L} \qquad \text{Eq. (27)}$$

To calculate the average heat transfer coefficient $\alpha_{i,R744}$ of the two-phase flow, a distinction is made between convective flow boiling and bubble boiling in chapter H3.4 of the VDI Heat Atlas. The model of convective flow boiling in horizontal pipes is used. This assumption is based on the low heat flux density when using the thermosiphon in the ice storage. For the calculation, the vapor mass fraction $\dot{x}$ and the density of the respective pure phase $\rho_{G/L}$ in $\mathrm{kg/m^3}$ are required.

$$\alpha_{i,R744} = \left\{ (1-\dot{x})^{0.01} \left[ (1-\dot{x}) + 1.2\dot{x}^{0.4} \left( \frac{\rho_L}{\rho_G} \right)^{0.37} \right]^{-2.2} + \dot{x}^{0.01} \left[ \frac{\alpha_G}{\alpha_L} \left( 1 + 8(1-\dot{x})^{0.7} \left( \frac{\rho_L}{\rho_G} \right)^{0.67} \right)^{-2} \right] \right\}^{-0.5} \cdot \alpha_L \qquad \text{Eq. (28)}$$

## 2.2. Simulation method

The equations described in chapter 2.1 are integrated into a Python program. With the help of the open source database "CoolProp" (Bell 2014), substance values for each operating condition can be retrieved automatically. As input parameters, the program requires the working medium, the transferred $\dot{Q}_{Ice}$ in W, the assumed evaporation temperature in °C, the inner pipe diameter $d_{pipe,a}$ in m and the wall thickness of the pipe $s_{pipe}$ in m, the diameter of the pipe coil $D_{Coil}$ in m and the distance of the coils from each other $h_{Coil}$ in m. The coil is thereby discretized into i steps of the vapor mass fraction $\dot{x}$. The accuracy of the results can be influenced by the step size.

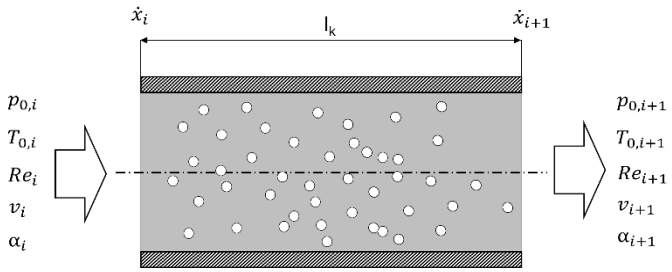


**Figure 5.1: Input and output parameters of a tube increment**

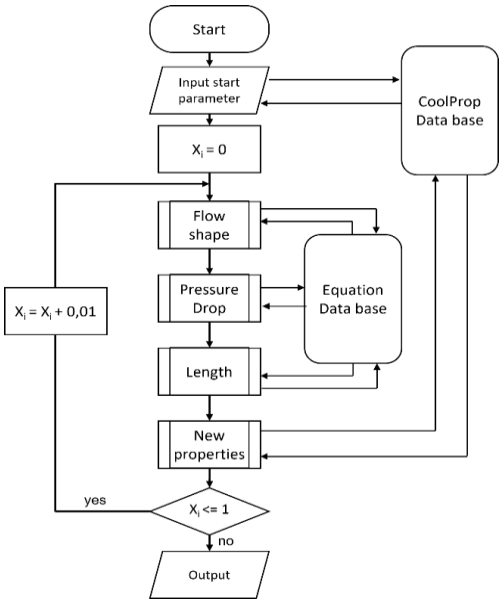


**Figure 5.2: Simulation flowchart**

Figure 5.1 shows the input and output parameters for one increment. For each pipe element of length $l_k$ in m, the thermodynamic state variables are calculated and assumed to be constant within one increment. The pressure losses are taken into account in the calculation of the subsequent increment. For all increments, flow shape, pressure loss, length and outlet conditions are determined. The calculation ends as soon as a vapor mass fraction $\dot{x} = 1$ is reached, which corresponds to the evaporation of the refrigerant. The simulation procedure is shown in Figure 5.2.

## 3. SIMULATION RESULTS

Before the pipe coil is simulated, a comparison of the models takes place using the example calculations in the corresponding chapters of the VDI Heat Atlas. After the calculations are validated by the comparison of the results, the coil geometry is implemented in the Python program. The simulation is performed at different pipe inner diameters $d_{pipe,i}$ and ice thicknesses $s_{ice}$. This is done to determine the tube length at which the required evaporator power $\dot{Q}_{ice}$ in W can be delivered even when the ice storage tank is partially loaded. The required length is then compared to the existing tube length of the tube coil. The existing pipe length is obtained from the assumed ice mass mice and the maximum intended ice thicknes. The literature (ASHRAE 2016) gives an ideal ice thickness of 36 mm, since the low thermal conductivity of ice $\lambda_{ice}$ makes a greater ice thickness inefficient. The input variables for the simulation can be found in Table 2.

**Table 2: Input values for simulation**

| Substance [-] | $\dot{Q}_{Ice}$ [W] | $T_{0,R744}$ [K] | $r_{pipe}$ [m] | $s_{pipe}$ [m] | $h_{Coil}$ [m] | $D_{Coil}$ [m] | $s_{ice}$ [m] | $m_{ice}$ [kg] |
|---|---|---|---|---|---|---|---|---|
| R-744 | 2000 | 268.15 | 0.005 | 0.002 | 0.08 | 0.4 | 0.036 | 205 |

First, the flow shape in the pipe segment is determined. The simulation results are shown in Figure 7. The smaller the inner pipe diameter, the fewer flow shapes are calculated over the pipe. One explanation is that with smaller diameter the velocity of the two-phase flow increases. As a result, the flow tends to take on more turbulent shapes, such as a surge, ring, and fog flow. With smaller diameters, the fog flow is achieved earlier. For diameters $d_{pipe,a}$ 6 mm, 8 mm and 14 mm, a wave flow is determined at the exit from the pipe. For large diameters, this is justified by the fact that the gas phase streams above the remaining liquid without entraining it. Due to the gradient angle Θ, the liquid runs back into the coil and a low liquid level is established in the outlet. However, for smaller diameters, the flow velocity are large enough to prevent a liquid level from forming. This is confirmed by the simulation results for the pipe diameters $d_{pipe,a}$ 10 mm and 12 mm. There, the expected fog flow forms at the outlet. Remaining liquid is entrained in droplet form by the high vapor flow velocity. Before the flow form assumes a fog flow, a surge flow is determined. The smaller the diameter, the longer the range of the surge flow. If the wave flow is also taken into account, this result can also be justified with the flow velocity of the two-phase flow. A higher gas velocity causes turbulence at the surface of the liquid resulting in a surge flow. For larger pipe diameters, this velocity is only reached at a higher vapor mass fraction $\dot{x}$. The flow forms are then considered for the pressure loss and heat transfer calculations.

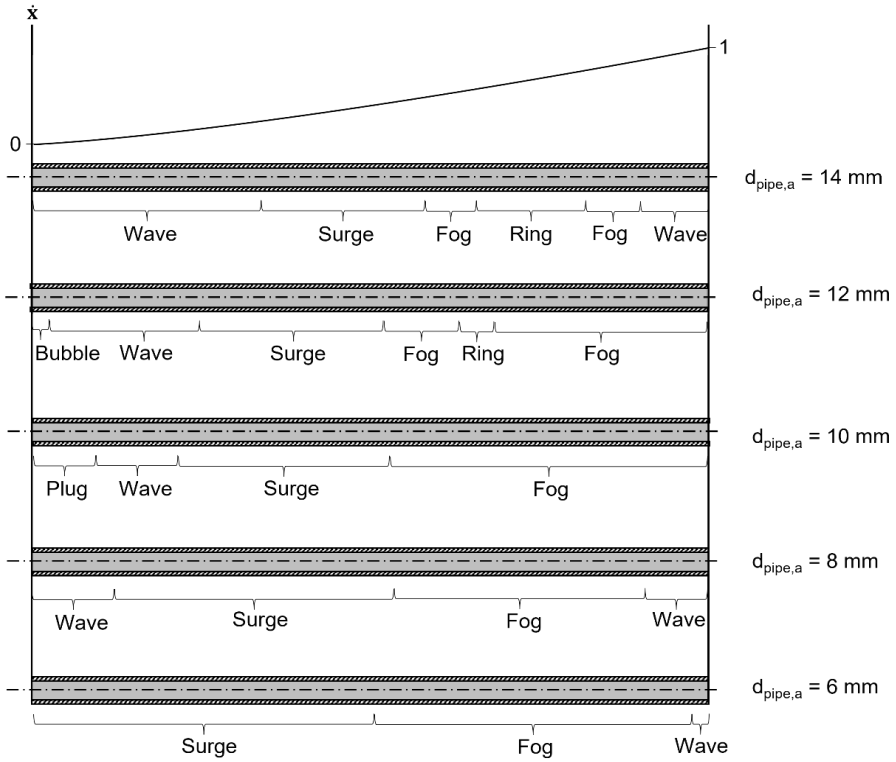


**Figure 7: Flow shapes at ice thickness $s_{ice}$ =36 mm and different pipe diameters**

For the following results, the different ice thicknesses are also integrated into the simulation. The simulation starts at an ice thickness $s_{ice}$ of 1 mm. After the calculations for a pipe from $\dot{x}$ = 0 to $\dot{x}$ =1 are completed, an ice growth $\Delta s_{ice}$ of 1 mm is calculated on the ice thickness. The simulation stops at a maximum thickness of 50 mm. The average heat transfer coefficient $\alpha_{R744}$ between the refrigerant and the surface of the tube is shown in Figure 8. For ice thicknesses $s_{ice}$ < 2 mm, the heat transfer coefficient decreases as the ice grows. Thereafter, the effect on the refrigerant-to-tube heat transfer coefficient is negligible. The choice of diameter, on the other hand, has a large effect on this parameter. The heat transfer coefficient is more than four times larger for the 6 mm tube, compared to twice the diameter 12 mm. However, if the averaged heat transmittance $K_{Péclet}$ is considered, it can be seen that larger inner diameters are advantageous. This is explained by the larger heat transfer area with larger outer diameters. With increasing ice thickness, this advantage diminishes and all heat transfer coefficients converge.

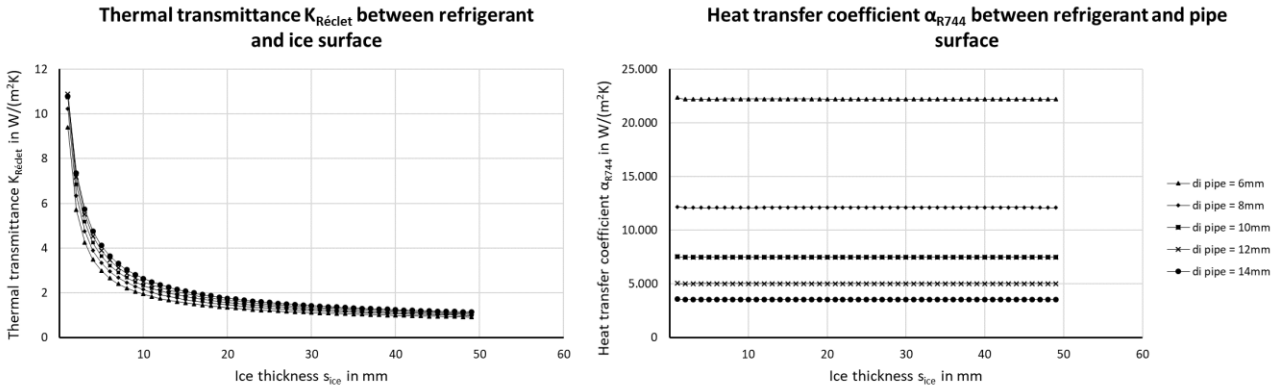


**Figure 8: Mean thermal transmittance (left) and mean heat transfer coefficient (right)**

Figure 9 shows the required tube lengths for different internal tube diameters $d_{pipe,a}$ and the required length through the ice mass. Using the intersection of the required length due to the ice mass and the length for the required evaporator capacity, the minimum required length can be determined. Since the tube is coiled with the pitch angle Θ (see Eq. 5), the height of the heat exchanger can be determined from the length of the tube.

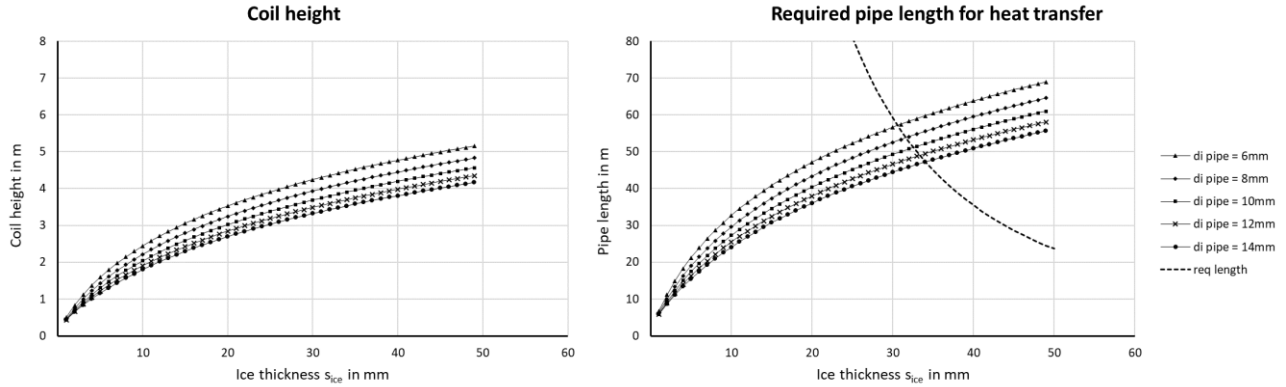


**Figure 9: Required coil length for growing ice layer at different pipe diameters**

Subsequently, the total pressure loss across the pipe helix $\Delta p_{2ph}$ is calculated. As shown in Eq. 12, this is composed of the friction pressure loss, the static pressure loss and the acceleration pressure loss. Figure 10 shows that if the diameter is greater than 10 mm the pressure loss depends only on the length of the coil. From this diameter, the friction and acceleration pressure losses are much smaller than the static pressure loss. The pressure loss is now compared to the installed pipe length and the resulting available pressure $p_s$. The friction pressure loss in the downpipe is calculated with the state variables at the inlet to the thermosiphon, where the refrigerant is still completely liquid, and the height of the coil (see Eq.1.1). In the right diagram it can be seen that for a pipe with an inner diameter $d_{pipe,a}$ of 6 mm, the natural circulation comes to a standstill at a pipe length of 42 m. However, since 59 m of pipe length is needed for the required ice mass, a larger inner diameter must be selected. To keep the refrigerant charge as low as possible, a tube with an inner diameter of 8 mm is recommended by the simulation. The driving pressure difference $\Delta p_{imp}$ with the required pipe length of 53.34 m is still 13415.5 Pa.

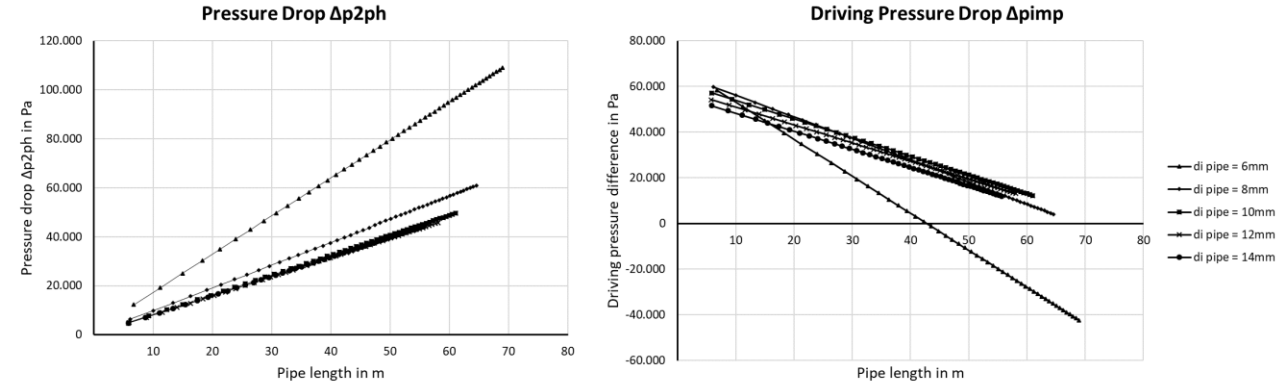


**Figure 10: Pressure drops at different pipe lengths and diameters**

## 4. CONCLUSIONS

The calculation modules of the simulation are validated by the example calculations from the literature. The simulation results of the thermosiphon show that a 54 m long pipe with an inner diameter of 8 mm can be used. Due to the low thermal conductivity of the growing ice layer, the mean heat transmittance decreases strongly up to an ice thickness of 10 mm. However, such a low ice thickness is very uneconomical, which is why the ice thickness of 36 mm suggested by the literature is targeted. The simulation results are used to dimension the natural circulation evaporator, which will be used in the EU project SophiA. Once the results from the thermosiphon test series are available, they will be compared with the simulation results.

## NOMENCLATURE

| | | | |
|---|---|---|---|
| $D$ | diameter (m) | $s$ | thickness (m) |
| $g$ | gravitational acceleration (m/s²) | $T$ | temperature (K) |
| $h$ | height (m) | $t$ | time (s) |
| $K$ | thermal resistance | $V$ | volume (m³) |
| $l$ | Length (m) | $w$ | Velocity (m/s) |
| $m$ | mass (kg) | $\dot{m}$ | mass flow density (kg/m²s) |
| $p$ | pressure (Pa) | $\dot{Q}$ | capacity (W) |
| $r$ | radius (m) | $\dot{x}$ | vapor mass fraction (-) |
| $\alpha$ | heat transfer coefficient (W/m²K) | $\xi$ | pressure loss coefficient (-) |
| $\gamma$ | transmission factor (-) | $\rho$ | density (kg/m³) |
| $\varepsilon$ | vapor volume fraction (-) | $\sigma$ | surface tension (kg/s²) |
| $\eta$ | dyn. Viscosity (kg/ms) | $\tau$ | angle (°) |
| $\lambda$ | heat conductivity coefficient (W/mK) | | |
| $Re$ | Reynolds number (-) | $Pr$ | Prandtl number (-) |
| $Fr$ | Froude number (-) | $Nu$ | Nusselt number (-) |
| $We$ | Weber number (-) | | |

## REFERENCES


ASHRAE, 2016. American Society of Heating, Refrigeration and Air-Conditioning Engineers, ASHRAE handbook: HVAC Systems and equipment. Chapter 51: Thermal Storage

Bell, I.H., Wronski, J., Quoilin, S., Lemort, V., 2014. Pure and Pseudo-pure Fluid Thermophysical Property Evaluation and the Open-Source Thermophysical Property Library CoolProp. Industrial & Engineering Chemical Research 53,6. p.2498 – p.2508

Garcia, F., Garcia, R., Padrino, J.C., Mata, C., Trallero, J.L., Joseph, D.D., 2003. Power law and composite power law friction factor correlations for laminar and turbulent gas-liquid flow in horizontal pipes. Int. Journal of Multiphase Flow Issue 29:1605–1624

Gnielinski, V., 2013. VDI-Wärmeatlas. G3 Durchströmte Rohrwendeln. Springer Vieweg, Berlin, Heidelberg. p.801 – p.803

International Energy Agency IEA, 2019. Africa Energy Outlook 2019. Paris. https://www.iea.org/reports/africa-energy-outlook-2019

Kauffeld, M., Eckert M., Siegismund V., 2022. Natural Refrigerants: Applications and Practical Guidelines VDE Verlag. LIV. 282 Pages. ISBN 978-3-8007-5330-7

Kind, M., 2013. VDI-Wärmeatlas. H3 Strömungssieden. Springer Vieweg, Berlin, Heidelberg. p.895 – p.1009

Maina, J., Ouma, P. O., Macharia, P. M., Alegana, V. A., Mitto, B., Fall, I. S., Noor, A. M., Snow, R. W., & Okiro. 2019. A spatial database of health facilities managed by the public health sector in sub Saharan Africa. https://doi.org/10.1038/s41597-019-0142-2 3

Martinelli, RC., Nelson, DB., 1948. Prediction of pressure drop during forced – circulation boiling of water. Trans ASME 70:695

Rouhani, Z., 1969. Modified correlations for void fraction and two-phase pressure drop. AB Atomenergi Sweden, AE-RTV-841

Schmidt, E. F., 1967. Wärmeübergang und Druckverlust in Rohrschlangen. Chemie Ingenieur Technik Vol. 39 p.781- p.789, https://doi.org/10.1002/cite.330391302

Strauss, K., 2016. Kraftwerkstechnik zur Nutzungfossiler, nuklearer und regenerativer Energiequellen. VDI Buch, Springer Verlag. 7. Auflage. 557 Pages. ISBN 978-3-662-53029-0

Wellenhofer A., Muschelknautz S., 2013 VDI-Wärmeatlas. L2.2 Druckabfall von Gas-Flüssigkeitsströmungen in Rohren, Leitungselementen und Armaturen Springer. Vieweg, Berlin, Heidelberg. p.1293 – p.1306